Hollowing Mechanism of Zinc Sulfide Nanowires in Vacuum Induced by an Atomic Oxygen Beam

Ming Lin,[†] Jia Zhang,[†] Chris Boothroyd,[‡] Yong Lim Foo,[‡] Mark Yeadon,[‡] and Kian Ping Loh*,[†]

Department of Chemistry, National University of Singapore, 3 Science Drive 3, Singapore 117543, and Institute of Materials Research and Engineering, 3 Research Link, Singapore 117602

The structural transformation of ZnS nanowires in high vacuum conditions induced by either atomic O beam treatment or electron beam irradiation has been studied. Interestingly, we observed that both types of treatments produce a higher rate of "hollowing" in the core of the wire than in its peripheral walls. Depending on the substrate temperature, atomic O beam treatment can either result in (i) the conversion of ZnS into ZnO nanotubules with similar dimensions due to incomplete structural relaxation or (ii) conversion into photoluminescent, nanocrystalline ZnO wires with dimensions much smaller than the starting ZnS nanowires. The observed morphological changes at different temperatures were due to the relative rate of evaporation of ZnS and its oxidation into thermally stable ZnO in the vacuum. Periodic density functional theory calculations were performed to derive insights into the contraction of the surface bonds and the unit cell volume following the substitution of S by O. Our calculations show that increasing the O content in the ZnS_xO_{1-x} alloy results in a monotonic decrease in the unit cell volume, while surface oxygenation leads to compressive stress, which is correlated to the elastic instability of the oxygenated ZnS nanowire.

1. Introduction

Nanowires[1−3] are of fundamental importance in the study of size-dependent chemical and physical phenomena. Under favorable reaction conditions, a nanowire may be used as a template for the formation of a new chemical phase of similar dimensions to the original nanowire.[4−6] Kinetically driven reactions may provide a valuable strategy to achieve this, since the resulting structures may differ substantially from the equilibrium phase. The strategy of morphology transfer from a dimensionally constrained template to a new chemical phase opens up a myriad of possibilities for the formation of core−shell or hollow tubule structures. Fundamentally, cylindrical nanowires present an interesting system for studying the evolution of reaction interfaces in a radial direction due to the inward-driven or outward-driven diffusion of atoms. The radial diffusion of atoms from the core to the periphery can, under the correct conditions, generate a void in the core, resulting in the formation of a tubule with no post-reaction etching required.

The electron beam induced degradation of zinc sulfide phosphor has been extensively studied due to the technological applications of zinc sulfide in field emission flat panel displays. It has been shown by Oosthuzien and co-workers[7] that, at an oxygen pressure of 1×10^{-6} Torr, an electron beam stimulates molecular oxygen into atomic species, resulting in the oxidation of ZnS into ZnO, leading to a reduction in cathodoluminescent efficiency. However, Choi[8] reported that encapsulating the ZnS with transparent, nanosized ZnO particles demonstrates excellent optical properties and prevents degradation from electron bombardment due to the relative stability of ZnO. In the present work, we investigate the effects of electron beam irradiation as well as atomic O beam treatment on the morphological transformation of ZnS nanowire *in a vacuum*. Interestingly, we observed a hollowing of the ZnS core brought about by such treatments and the formation of ZnO nanotubules as well as optically active ZnO nanocrystalline wires at different processing temperatures. The mechanism of morphology transfer from ZnS into ZnO nanowires will be discussed.

2. Experimental Section

Supported Au nanoclusters were prepared by electron beam evaporation of a 10 nm thick Au film onto a Si(100) wafer, followed by thermal annealing. ZnS nanowires were grown by thermally evaporating 1 g of ZnS powder under a dynamic vacuum of 1×10^{-5} Torr. The powder was evaporated from a high-temperature Knudsen cell operated at 1000 °C, onto the Au-coated silicon substrate, with the substrate temperature maintained at 700 °C. Atomic oxidation of the ZnS nanowires was performed in a ultrahigh vacuum system equipped with a remote discharge, 13.56 MHz radio frequency oxygen atom beam source (Oxford Applied Research). Atomic O beam irradiation of the sample was performed at a background pressure of 1×10^{-4} Torr and with two substrate temperatures, 500 and 700 °C. The treatment time was around 30 min. Transmission electron microscopy (TEM) was performed using a 300-kV Philips CM300. The in situ TEM study of ZnS was carried out in a 200-kV JEOL JEM 2000V transmission electron microscope. This microscope has a base working pressure of 1×10^{-9} Torr and is equipped with in situ heating and gas injection capabilities together with an electron energy filter (GIF) for chemical microanalysis.

The density functional theory (DFT) calculations were performed using the CASTEP program code, in which a plane-

* To whom correspondence may be addressed. E-mail: chmlohkp@nus.edu.sg (K.P.L.).
† National University of Singapore.
‡ Institute of Materials Research and Engineering.

wave basis set was used.[9] In the present study, the electron−ion interactions were described using ultrasoft pseudopotentials.[10] The geometry optimizations were performed by the Broyden−Fletcher−Goldfarb−Shanno routine.[11] The exchange and correlation energies were calculated with the Perdew−Wang form of the generalized gradient approxomation.[12] Special k-point meshes used for Brillouin-zone integration were generated by the Monkhorst−Pack scheme.[13] The plane-wave cutoff energy was set at 400 eV. The equilibrium lattice constants of $a = 3.821$ Å and $c = 6.260$ Å were obtained by optimizing the unit cell of bulk wurtzite ZnS. These values are in good agreement with experimental data ($a = 3.80$ Å and $c = 6.23$ Å), with an error of less than 0.55%. A symmetric 8-atom wurtzite supercell was constructed to model the ZnS bulk crystal. To calculate the lattice contraction, the sulfur atoms were substituted by O to form an alloyed ZnS_xO_{1-x}. The equilibrium geometries were calculated by fixing the values of the unit cell edge angles α, β, and γ and optimizing the other cell parameters.

The supercell method was used to calculate the surface structure. Two models were constructed in this study for comparison: (a) the wurtzite S-terminated ZnS (0001) surface and (b) the wurtzite O-substituted ZnS (0001) surface model in which the S atoms of the top two bilayers are replaced by O atoms. Five bilayers of ZnS were considered in the calculation, and each bilayer consists of Zn and S atomic layers. The bottom Zn atoms were saturated with OH. A 10-Å vacuum was introduced between the five-bilayer simulation slabs to ensure the isolation of the slabs.

3. Results and Discussion

A scanning electron microscope (SEM) image of the ZnS nanowires grown by thermal evaporation of ZnS powder is presented in Figure 1a. The diameters of the wires were found to be between 80 and 100 nm, with typical lengths of ∼10 μm. The classical vapor−liquid−solid growth mechanism[14] is responsible for wire formation, with the nucleation of ZnS nanowires occurring on Au−Zn−S alloy nanoclusters formed on the substrate.

From X-ray diffraction (XRD) (Figure 2a), the structure was determined to be entirely hexagonal wurtzite polytype, with lattice constants $a = 0.380$ nm and $c = 0.623$ nm, in good agreement with the Joint Committee on Powder Diffraction Standards (JCPDS) 75-1534 database.[15] The internal microstructure was further examined by TEM. Figure 3a shows a high-resolution image of a ZnS nanowire, along with the corresponding electron-diffraction pattern (inset). The lattice fringes in the image have a spacing of 0.33 nm, which corresponds to the {100} planes of ZnS. This therefore shows that the growth direction of the wires occurs along the (100) normal.

Atomic oxidation of the ZnS nanowires was subsequently performed, at a background pressure of 1×10^{-4} Torr using an oxygen atom beam source. At a substrate temperature of 700 °C, complete oxidation of the single crystalline ZnS nanowires to nanocrystalline ZnO nanowires was observed after 30 min of oxidation. An SEM image of the resulting ZnO, shown in Figure 1b, demonstrates that the ZnO is in the form of nanowires and therefore a successful morphology transfer has occurred. We note that the width of the nanowire has reduced visibly by at least 20 nm to ∼60 nm. This is consistent with the reduction in unit cell volume following conversion into ZnO. Our periodic DFT calculation (discussed below) shows a progressive reduction in the unit cell volume following the alloying of ZnS with increasing concentration of O. However, when the oxidation
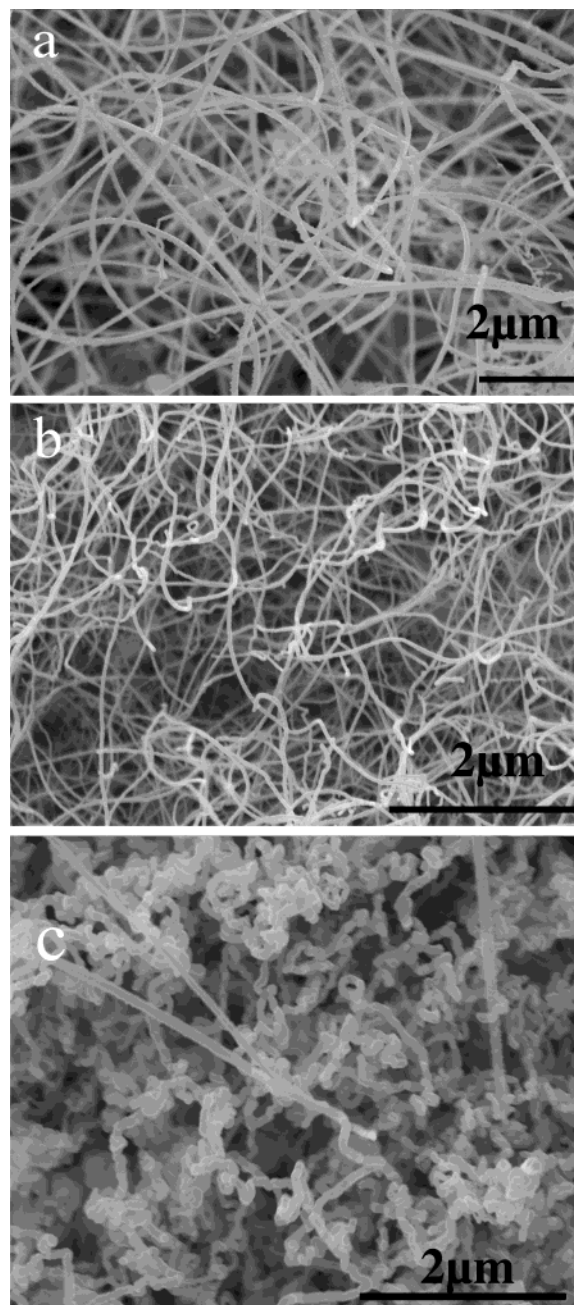
Figure 1. SEM images of (a) ZnS nanowires, (b) ZnO nanowires after oxidation at 700 °C, and (c) ZnO nanotubes after oxidation at 500 °C.

temperature of the ZnS nanowire was reduced to 500 °C, the post-oxidation external dimensions were similar to those of the original ZnS nanowire, as shown in Figure 1c, due to incomplete structural relaxation at this lower temperature.

Figure 2b shows the XRD spectrum of the products following atomic O beam oxidation of the ZnS nanowire at 500 °C. The pattern is similar to that of wurtzite ZnS, suggesting that the oxidation is not complete, and the oxygenated phase, if present, is not crystalline. After the oxidation of the ZnS nanowire at 700 °C however, there is a complete transformation of the XRD pattern to that consistent with hexagonal wurtzite ZnO, with $a = 0.325$ nm and $c = 0.521$ nm (JCPDS 36-1451). A high-resolution TEM image of one of these nanowires, shown in Figure 3b, reveals the nanowire to be composed of ZnO nanocrystals with an average diameter of ∼6 nm. Two sets of resolved fringes, with interplanar spacing of 0.28 and 0.26 nm, corresponding to the (100) and (002) planes of ZnO are

Hollowing Mechanism of Zinc Sulfide Nanowires

J. Phys. Chem. B, Vol. 108, No. 28, 2004 **9633**
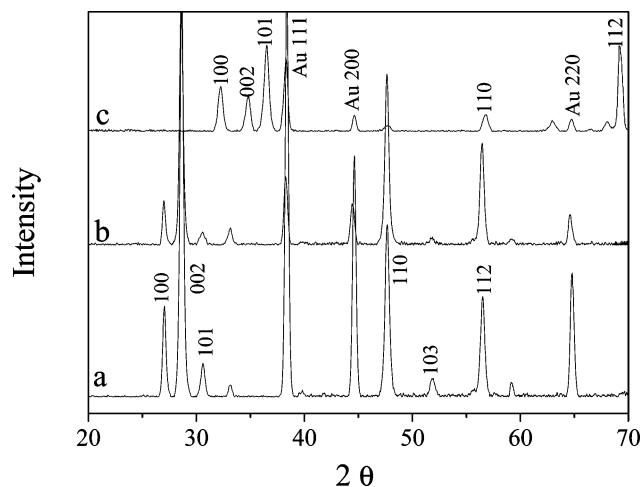
Figure 2. X-ray spectra of (a) original ZnS nanowires with wurtzite structure, (b) the same after atomic O treatment at 500 °C, and (c) transformation into ZnO nanowires after atomic O treatment at 700 °C.
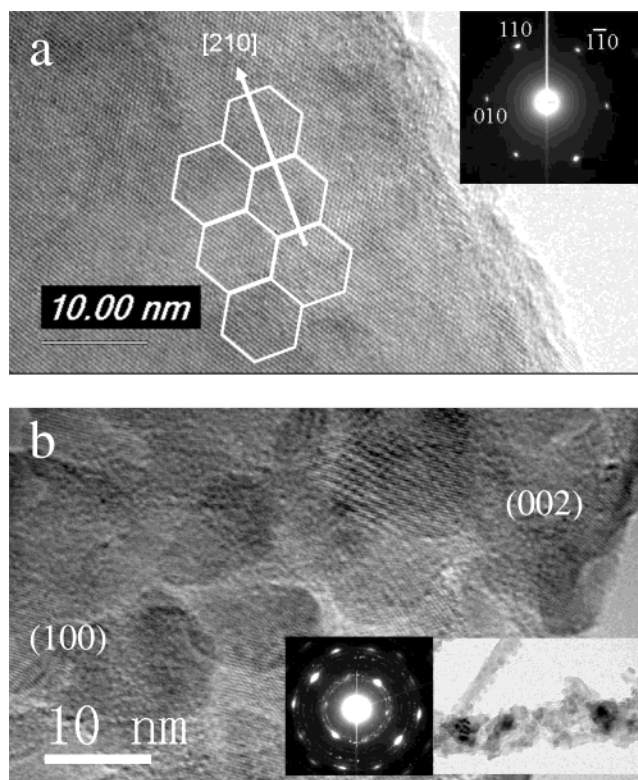
Figure 3. TEM images of (a) ZnS nanowire taken with the beam along [001], showing the growth axis as [210] and (b) ZnO nanograins in a ZnO nanowire with insets showing nanocrystalline grains at low magnification and a diffraction pattern.

highlighted in Figure 3b. The corresponding electron-diffraction pattern is shown in the inset.

To gain an insight into the reactive interface formation in the atomic O beam oxidation process, the substrate temperature during oxidation was lowered to 500 °C to see if a partially oxidized structure consisting of a core of ZnS and an outer shell of ZnO can be formed. We found that, at a lower temperature, a transformation of the original compact ZnS wire morphology into a ZnO nanotube structure occurred. Although the XRD spectrum of the sample at this stage revealed only peaks due to ZnS (Figure 2b), electron energy loss spectroscopy of the nanowire reveals they are in fact amorphous ZnO nanowires grown on a crystalline ZnS bulk. An SEM image of the ZnO
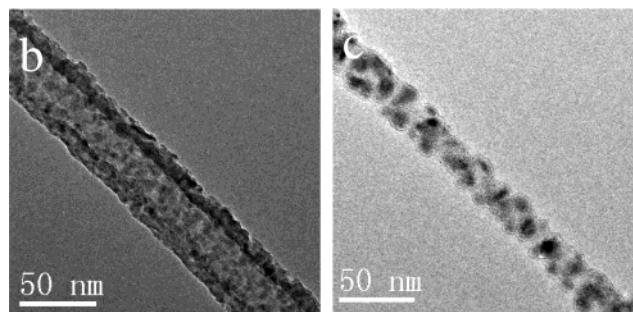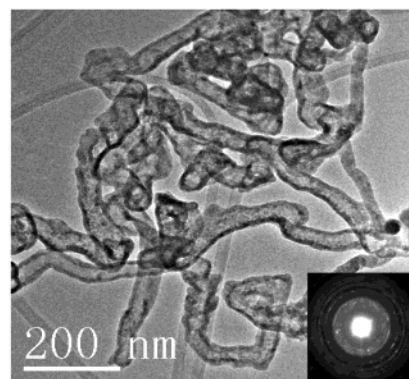
Figure 4. (a) ZnO nanotubules at low magnification, (b) ZnO nanotubules at high magnification showing suspended ZnO nanocrystals in the core, and (c) ZnO nanotube after intense 300-keV beam irradiation.

nanotubule in Figure 1c shows a twisted, convoluted structure, as opposed to the straight, belt-like ZnS nanowire in Figure 1a. Figure 4a shows a TEM image of the nanotubules, where the formation of a hollow core can be observed together with a highly convoluted structure. We suggest that the driving force for this shape change arises from the lateral contraction of surface bonds following the substitution of S by O, this produces compressive stress which induces bucking or elastic instability of the tubular structure. The polycrystalline nature of the nanotubule can be judged from the diffraction pattern in the inset. A high-magnification TEM image in Figure 4b shows numerous ZnO nanocrystals suspended in the nanotubule, with diameters ranging from 2 to 5 nm.

Elemental mapping using the zinc L, oxygen K, and sulfur L energy-loss edges was done to determine the compositional uniformity of the nanotubes and the maps are shown in Figure 5. Unfortunately, ZnO damages readily under the high-electron doses required for these images, and the resulting distortions of the ZnO tube manifest themselves in a poor alignment of the three images from which the elemental maps are formed. Nevertheless, it can be seen that oxygen is uniformly distributed throughout the nanowire and that sulfur is present at only low concentrations. Interestingly, a number of bright spots are present only in the Zn image suggesting local nonstoichiometry.

To evaluate the optical quality of the nanowires at different stages of treatment, room-temperature photoluminescence (PL) spectra (325-nm line of a He–Cd laser) were recorded. For the original ZnS nanowire, only a broad green peak at 515 nm is present as shown in Figure 6a, this has been previously associated with the Au–Zn–S luminescent center.[16] Figure 6b shows the room-temperature PL spectra of the nanocrystalline ZnO nanowires produced by atomic O beam treatment at 700 °C. A single peak at 380 nm, due to free-exciton recombination,[17] can be seen. The absence of defect-related peaks suggests that the ZnO nanocrystals obtained by atomic O beam treatment
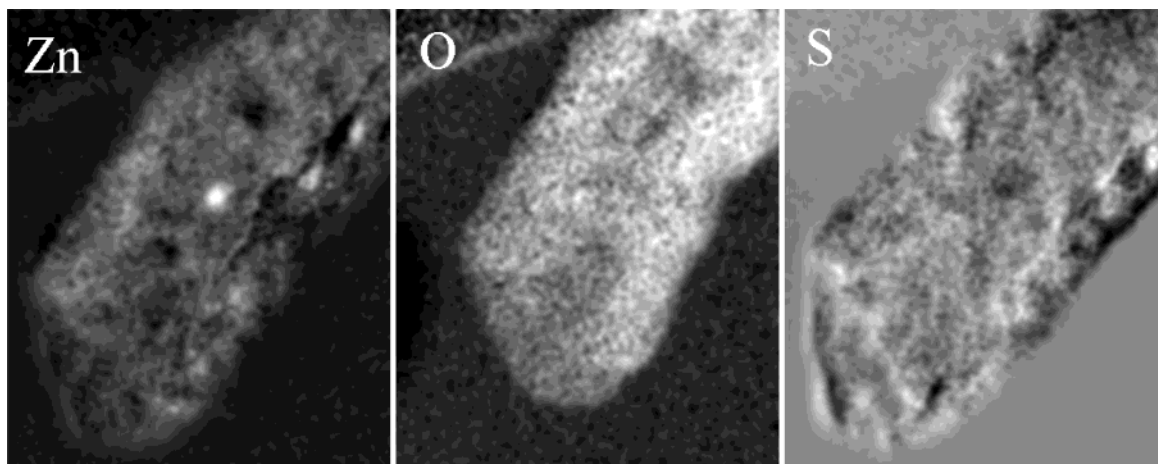
Figure 5. Energy-filtered maps of a ZnO nanotubule using the (a) Zn L, (b) O K, and (c) S L edges.
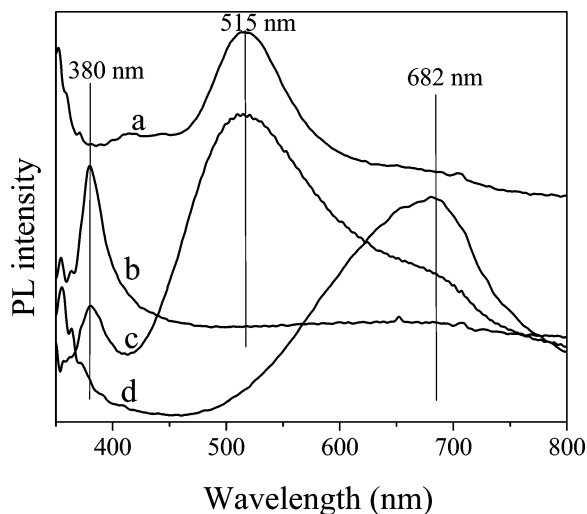
Figure 6. PL spectra of the (a) ZnS nanowires, (b) ZnO nanowires after atomic oxygen oxidation at 700 °C, (c) ZnO nanowires after molecular oxidation at 700 °C, and (d) ZnO nanotubules after atomic oxygen oxidation at 500 °C.

are of high-quality, with few vacancies or interstitial-related traps. Therefore at 700 °C, atomic O can effect a highly efficient conversion of ZnS into ZnO. In comparison, experiments on the molecular oxidation of ZnS nanowires at a pressure of 10 Torr reveal that the resultant ZnO wires have more defects. This is demonstrated by the corresponding PL spectrum shown in Figure 6c, which shows that, in addition to the exciton peak, broad peaks at 510 and 680 nm[18,19] are present, which may be attributed to singly ionized oxygen vacancies and interstitial zinc. The reaction efficiency of atomic O with ZnS nanowires is much higher than with molecular O_2 since predissociation is not needed, and direct diffusion into the ZnS matrix can occur. The PL spectra of the ZnO nanotubules produced by atomic oxidation at 500 °C is shown in Figure 6d, where a strong defected-related emission at 682 nm due to interstitial zinc can be seen.[18,19]

Our studies show that two types of products are obtained here following atomic O beam treatment of the ZnS nanowire, depending on the temperature. At the higher temperature of 700 °C, there is a transformation into excitonically active nanocrystalline ZnO wires, with a notable reduction in diameter compared to the original ZnS nanowires. In comparison, at a temperature of 500 °C, a hollowing of the core to form ZnO nanotubules occurs. We propose a mechanism to explain the different reaction products based on the competing rate between

the oxidation and evaporation of ZnS in a vacuum. ZnS has a partial vapor pressure of 10^{-4} Torr at 800 °C and atmospheric conditions, whereas ZnO requires temperatures in excess of 1800 °C to reach the equivalent partial pressures. At 700 °C, atomic O can diffuse rapidly into the ZnS nanowire to produce complete oxidation of the wire and prevent its evaporation. Our periodic DFT calculations of the bulk structure show that there is a contraction in the average unit cell volume following the alloying of ZnS with increasing concentrations of O to form ZnS_xO_{1-x}. Figure 7 shows the equilibrium geometries of the ZnS_xO_{1-x} after the progressive substitution of S atoms by O atoms. The structural parameters around the substituted O atoms are highlighted. It is found that both the length of the Zn−O bond and the Zn−O−Zn bond angle decreases as O is substituted into ZnS. Such a distortion of the lattice introduces considerable tensile stress, which is relieved by the breakup of the lattice into ZnO nanocrystals. Numerous voids are created when the lattice breaks and contracts, these will facilitate the further diffusion of oxygen into the core and enhances the oxidation process. If there is no thermal evaporation of ZnS, then the nanowire diameter would be expected to contract by 20% on complete oxidation to ZnO.

At 500 °C, the diffusion of O into the bulk of the ZnS nanowires is slower. In this case, the oxidation is limited to the outer walls at first to form a ZnO shell, which is thermally more stable than ZnS at this temperature. Because of the slower rate of inward oxidation, the ZnS in the core evaporates at 500 °C in a vacuum to leave voids, thus producing a nanotubule with a ZnO shell. The diameter of the ZnO nanotubule is similar to the initial ZnS nanowire from which it is derived because complete structural relaxation is prevented at this temperature. Figure 8 shows a side view of the surface slabs of the optimized S-terminated (0001) ZnS surface and the O-substituted (0001) ZnS surface. The surface-slab calculations reveal that the replacement of S by the more electronegative O on the surface results in a bond contraction of around 6% for Zn−O bonds parallel to the surface and a 17% reduction in the O−Zn bond lengths pointing inward. The growth of thicker ZnO layers on ZnS will result in a buildup of compressive stress on the surface, this manisfests in the buckling and curling of the ZnO nanotubules, as seen in Figure 1c.

When the ZnO nanotubules are subjected to high-energy electron beam irradiation, they readily change to form a loose agglomeration of ZnO nanocrystals while maintaining the outward morphology of a wire. The diameter of the beam-damaged ZnO nanotubules is reduced by almost 40% when compared to the original ZnS nanowires. This is seen from the

Hollowing Mechanism of Zinc Sulfide Nanowires

J. Phys. Chem. B, Vol. 108, No. 28, 2004 **9635**
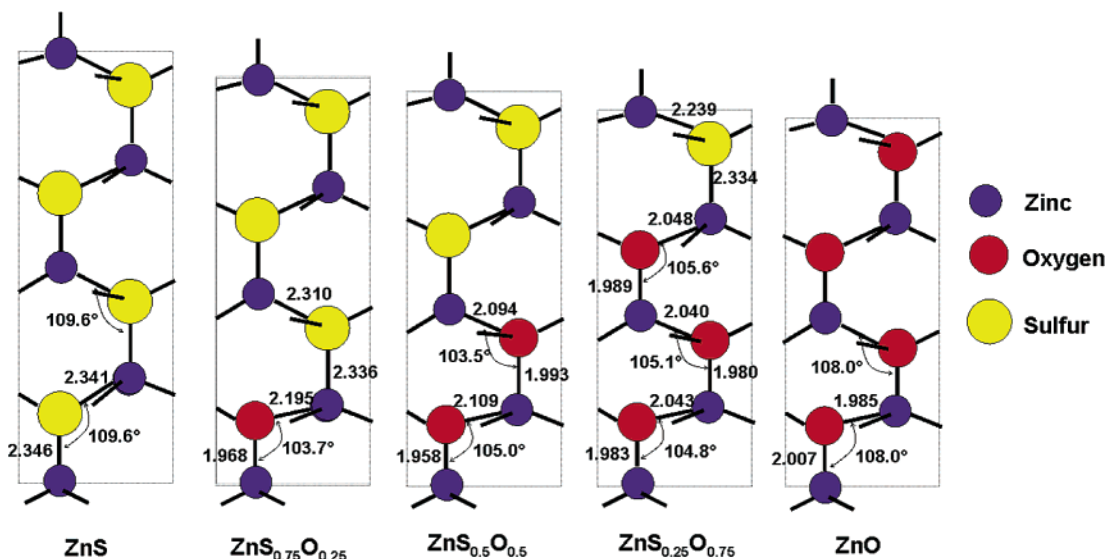
Figure 7. Structural models of ZnS_xO_{1-x} with bond lengths (Å) and angles marked. Note that the unit cell becomes progressively smaller with increasing O substitution.
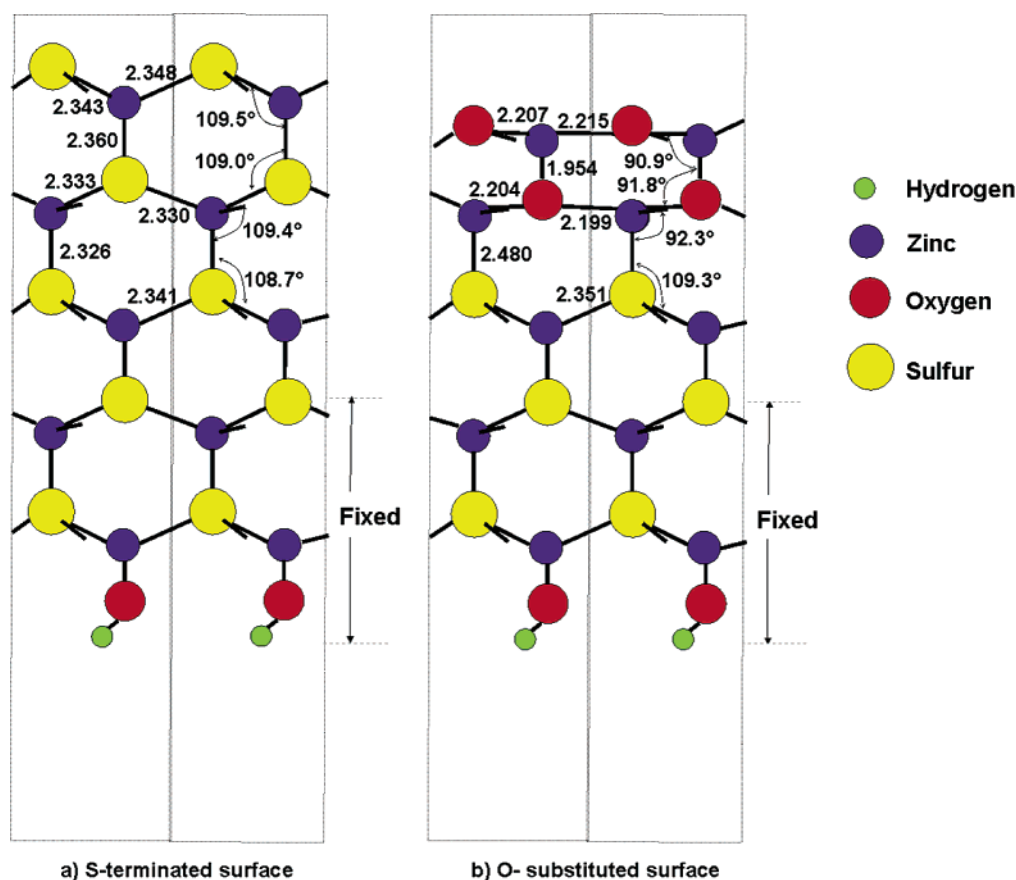
Figure 8. Side views of the surface slabs of (a) the optimized S-terminated (0001) ZnS surface and (b) the O-substituted (0001) ZnS surface, with two oxygen layers. The bond lengths are given in Å.

TEM image of a beam-damaged ZnO nanocrystalline wire shown in Figure 4c, generated from a ZnO nanotubule after 300-keV electron beam irradiation. Our results suggest the possibility of using a two-step strategy to restructure the diameter of the nanowire template. ZnO nanotubules can be generated from a ZnS nanowire template by oxidation, followed by a second structural relaxation process to collapse the voids to form a more compact but considerably thinner nanocrystalline ZnO wire. This structural relaxation can be achieved by annealing the ZnO nanotubule at a higher temperature in oxygen,

which can have the added advantage of annealing out the defects in the nanocrystalline ZnO wire to form photoluminescent, nanocrystalline ZnO wire.

The formation of nanotubes from ZnS nanowires can also occur by electron beam irradiation under oxygen-free conditions. Figure 9 shows a series of TEM images taken as a function of time, while a ZnS nanowire is being irradiated with 200-kV electrons in a background pressure of 1×10^{-8} Torr and a temperature of 300 °C. Bright field images were taken every 5 s to record the structural changes taking place during the heating
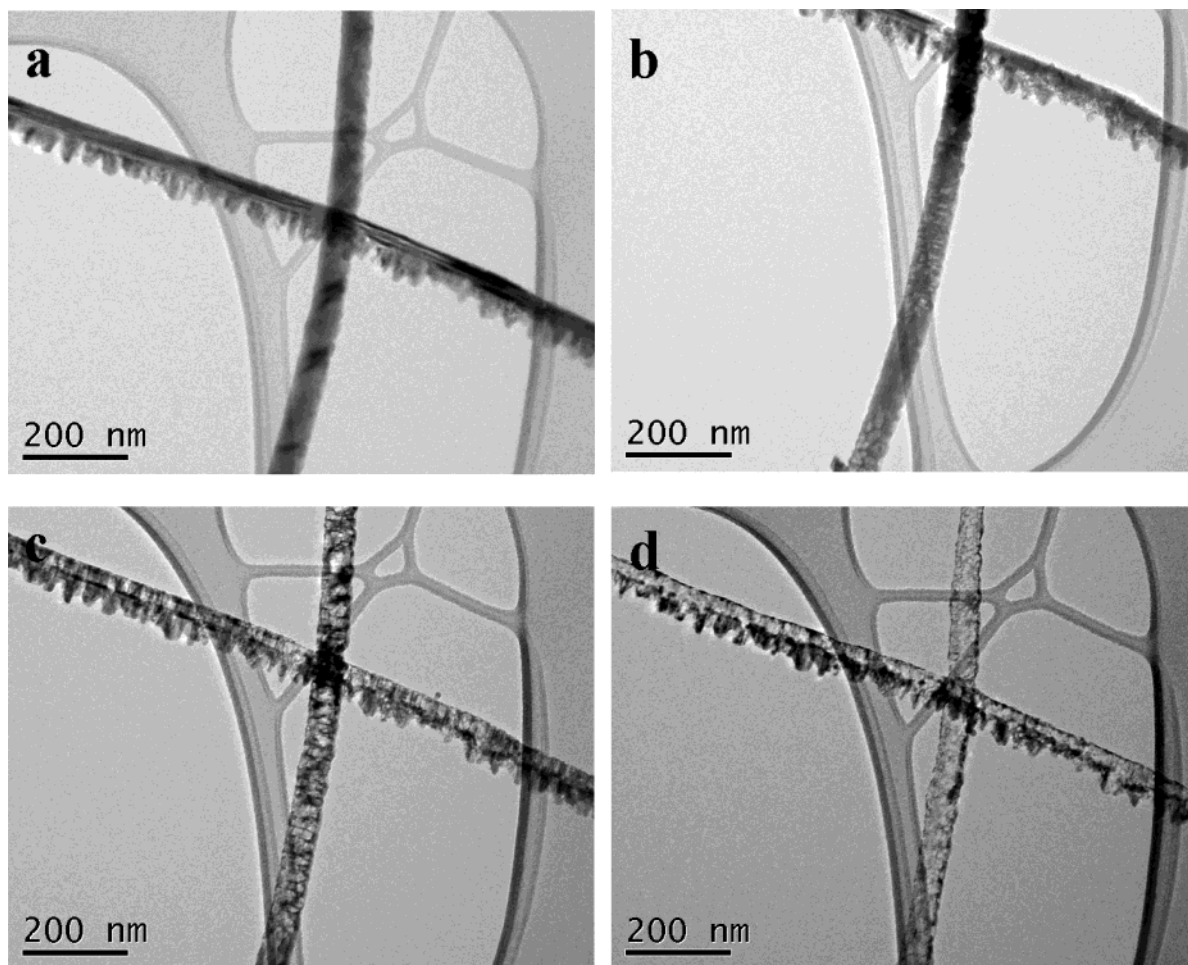
Figure 9. TEM images of ZnS nanowires after annealing in situ for (a) 0, (b) 400, (c) 1020, and (d) 1500 s.

process, and images recorded after 0, 400, 1020, and 1500 s are shown in Figure 9. It can be seen that the ZnS nanowire becomes increasingly porous with increasing electron beam irradiation time, while the edges of the nanowire remain seemingly intact. This transformation only occurred when the sample was heated at 300 °C and the electron beam was irradiated simultaneously.

Interaction with charged particles can produce various effects on the material being irradiated. For small energy transfers, electronic excitation of valence electrons into the conduction band creates excited states. Excited states can lead to local chemical modification by atomic-bonding instabilities and rearrangement. ZnO nanocrystals have previously been observed to form from ZnS by electron beam irradiation.[20] In addition, ZnO is known to damage under an electron beam by the release of O, leaving behind Zn.[21] The relative stability of the peripheral regions compared to the core may be due to the presence of a thermally more stable ZnO layer present as an outer sheath on the ZnS. X-ray photoelectron spectroscopy of the original ZnS nanowires shows the presence of surface oxides on the wire, and we attribute this to the room-temperature oxidation of the ZnS surface. The surface oxide protects the peripheral regions from electron beam degradation. This hollowing process further proves the oxidation mechanism proposed above. Atomic O in the gas-phase diffuses into the peripheral regions and effects a conversion of this region into a crystalline ZnO shell. The ZnS in the core evaporates in high vacuum and this results in material loss from the core. The outer shell of ZnO is stable in the oxidizing environment and acts as a reverse template for the deposition of ZnO from volatile ZnS vapor and oxygen atoms.

Therefore, there is an outward-driven radial movement of ZnS onto the inner face of the ZnO shell to form ZnO, contributing to the hollowing out of the core.

4. Conclusions

In summary, we have shown that direct morphology transfer between ZnS nanowires and nanocrystalline ZnO nanowires or nanotubes can be obtained by atomic O beam treatment under high vacuum conditions. The ZnO nanocrystalline wires are optically active, with exciton-derived room-temperature PL following atomic O beam induced conversion at 700 °C. A lowering of the oxidation temperature favors the formation of ZnO nanotubes, which provide a one-dimensional scaffold for the suspension of very fine ZnO nanocrystals at the core. The "hollowing" process of ZnO nanotubule formation, followed by structural relaxation during high temperature annealing, can potentially provide an effective strategy to form very thin nanocrystalline ZnO nanowires. The conversion of ZnS nanowires to ZnO provides us with a new perspective to understand the oxidation mechanism of ZnS and the stability of ZnS phosphors under electron beam irradiation in a vacuum. ZnO nanocrystalline wires may show interesting properties as an active random medium in stimulated UV lasing, which will be the subject of further investigations.

References and Notes

(1) Park, W. I.; Yi, G. C.; Kim, M.; Pennycook, S. J. *Adv. Mater.* **2003**, *15*, 526.
(2) Reynolds, D. C.; Look, D. C.; Jogai, B.; Collins, T. C. *Phys. Rev. B* **1997**, *56*, 13753.

(3) Huang, M. H.; Mao, S.; Feick, H.; Yan, H. Q.; Wu, Y. Y.; Kind, H.; Weber, E.; Russo, R.; Yang, P. D. *Science* **2001**, *292*, 1897.

(4) Wang, X. D.; Gao, P. X.; Li, J.; Summers, C. J.; Wang, Z. L. *Adv. Mater.* **2002**, *14*, 1732.

(5) Dloczik, L.; Engelhardt, R.; Ernst, K.; Fiechter, S.; Sieber, I.; Konenkamp, R. *Appl. Phys. Lett.* **2001**, *78*, 3687.

(6) Wu, J. J.; Liu, S. C.; Wu, C. T.; Chen, K. H. *Appl. Phys. Lett.* **2002**, *81*, 1312.

(7) Oosthuizen, L.; Swart, H. C.; Viljoen, P. E.; Holloway, P. H.; Berning, G. L. P. *Appl. Surf. Sci.* **1997**, *120*, 9.

(8) Choi, H.-H.; Ollinger, M.; Singh, R. K. *Appl. Phys. Lett.* **2003**, *82*, 2494.

(9) Payne, M. C.; Teter, M. P.; Allan, D. C.; Arias, T. A.; Joannopoulos, J. D. *Rev. Mod. Phys.* **1992**, *64*, 1045.

(10) Vanderbilt, D. *Phys. Rev. B* **1990**, *41*, 7892.

(11) Polak, E. *Computational Methods in Optimization*; Academic: New York, 1971; p 56ff.

(12) Perdew, J. P.; Wang, Y. *Phys. Rev. B* **1992**, *45*, 13244.

(13) Monkhorst, H. J.; Pack, J. D. *Phys. Rev. B* **1976**, *13*, 5188.

(14) Gudiksen, M. S.; Lauhon, L. J.; Wang, J.; Smith, D. C.; Lieber, C. M. *Nature* **2002**, *415*, 617.

(15) Kiang, Y.; Meng, X. M.; Lin, J.; Xie, Z. Y.; Lee, C. S.; Lee, S. T. *Adv Mater.* **2003**, *122*, 323.

(16) Wang, Y. W.; Zhang, L. D.; Wang, G. Z.; Peng, X. S. *Chem. Phys. Lett.* **2002**, *357*, 314.

(17) Srikant, V.; Clarke, D. R. *J. Appl. Phys.* **1998**, *83*, 5447.

(18) Spanel, L.; Anderson, M. A. *J. Am. Chem. Soc.* **1991**, *113*, 2826.

(19) Vanheusden, K.; Seager, C. H.; Warren, W. L.; Tallant D. R.; Voight, J. A. *Appl. Phys. Lett.* **1996**, *68*, 403.

(20) Kogure, T.; Bando, Y. *J. Electron Microsc.* **1998**, *47*, 135.

(21) Devenish, R. W.; Bullough, T. J.; Turner, P. S.; Humphreys, C. J. *Inst. Phys. Conf. Ser.* **1990**, *98*, 215.